Strahlentherapie
und Onkologie

Review Article

Aspects of MR Image Distortions in Radiotherapy Treatment Planning

Annette Fransson[1], Pedro Andreo[2], Richard Pötter[1]

Background: Registration of computed tomography (CT) and magnetic resonance (MR) images are commonly performed to define the different target regions used in radiotherapy treatment planning (RTTP). The accuracy of target definition will then depend on the spatial accuracy of the CT and MR data, and on the technique used to register the images. CT images are usually regarded as geometrically correct, while MR images are known to suffer from geometric distortion. The aim of this paper is to discuss the possible impact of MR image distortions in the radiotherapy treatment planning process.
Methods: The origin, magnitude, and relative impact of the different sources of geometric distortions that affect the MR image data at different magnetic fields and for different acquisition settings are described. Techniques for distortion correction are reviewed, and their limitations are outlined. The sensitivity of image registration techniques to the presence of geometric distortions in the MR data is discussed. Finally, an overview of image registration techniques used and results obtained in clinical radiotherapy treatment planning applications is given.
Results: Spatial distortions in MR images vary with field strength and with the image acquisition protocol. The spatial accuracy generally decreases with distance from the magnet isocenter. Distortion correction techniques based on phantom evaluations cannot adequately model patient-induced distortions.
Conclusion: Image protocols with high gradient bandwidths should be used to reduce the spatial distortions in MR images. Correction techniques based only on phantom measurements could be sufficient at low magnetic fields, while at higher fields additional corrections of patient-related distortions might be needed. Registration techniques based on matching of landmark points located far from the magnet isocenter are especially prone to MR distortions.

Key Words: Magnetic resonance imaging · Geometric distortion · Radiotherapy treatment planning · Image registration

Strahlenther Onkol 2001;177:59–73
DOI 10.1007/s00066-001-0771-0

Aspekte der Verzeichnung von MRT-Bildern für den Planungsprozess in der Radiotherapie

Hintergrund: Die Registrierung von CT- und MR-Bildern erfolgt, um die unterschiedlichen Zielgebiete für die Planung der Radiotherapie zu definieren. Die Genauigkeit der Zielvolumendefinition ist abhängig von der räumlichen Genauigkeit der CT- und MRT-Daten und von der Technik der Datenregistrierung. CT-Bilder werden üblicherweise als geometrisch korrekt angesehen, während bei MR-Bildern geometrische Verzeichnungen bekannt sind. Die Zielsetzung dieser Arbeit liegt darin, die mögliche Bedeutung von Verzeichnungen der MRT für die Planung der Radiotherapie zu diskutieren.
Methoden: Der Ursprung, der Umfang und die entsprechende Bedeutung der verschiedenen Quellen geometrischer Verzeichnungen werden beschrieben, die MR-Bilder bei unterschiedlichen Magnetfeldern und Akquisitionen beeinflussen. Ein Überblick über die Korrekturmöglichkeiten für derartige Verzeichnungen wird gegeben, wobei insbesondere die Grenzen dieser Korrekturmöglichkeiten dargestellt werden. Die Sensitivität der Techniken für die Bildregistrierung im Hinblick auf vorhandene geometrische Verzeichnungen der MR-Daten wird diskutiert. Schließlich erfolgt ein Überblick über die heute verfügbaren Techniken der Bildregistrierung und der Ergebnisse, die erzielt werden, wenn derartige Techniken für die klinische Radiotherapieplanung angewendet werden.
Ergebnisse: Räumliche Verzeichnungen von MR-Bildern variieren mit der Feldstärke und dem Akquisitionsprotokoll für die Bilderstellung. Üblicherweise nimmt die räumliche Genauigkeit mit der Entfernung vom Isozentrum des Magneten ab. Techniken zur Korrektur der Verzeichnungen, die auf Phantommessungen beruhen, können die im Patienten entstehenden Verzeichnungen nicht adäquat berücksichtigen.

[1] Department of Radiotherapy and Radiation Biology, University Hospital – AKH, Vienna, Austria,
[2] Dosimetry and Medical Radiation Physics Section, Division of Human Health, IAEA, Vienna, Austria.

Submitted: February 24, 2000; accepted: August 10, 2000.

Schlussfolgerung: Zur Reduktion der räumlichen Verzeichnungen bei MR-Bildern sollten Protokolle zur Bilderstellung benutzt werden, die über eine große Bandbreite der Gradienten verfügen. Bei Magneten niedriger Feldstärke sind Korrekturprogramme ausreichend, die auf Phantommessungen beruhen, während bei höheren Feldstärken zusätzliche Korrekturen notwendig sein dürften, die im Patienten entstehende Verzeichnungen mit berücksichtigen. Techniken der Bildregistrierung, die sich auf das „Matchen" von Referenzpunkten beziehen, die weit vom Isozentrum des Magneten entfernt sind, sind besonders anfällig für MR-Verzeichnungen.

Schlüsselwörter: Magnetresonanztomographie · Geometrische Verzeichnung · Planungsprozess in der Radiotherapie · Bildregistrierung

Introduction

One of the major concerns in radiation therapy treatment planning (RTTP) is to define accurately the gross tumor volume (GTV) [20] and its topographic relationship to organs at risk. A distinct, three-dimensional, description of the gross tumor volume combined with refined techniques for treatment delivery will allow for an optimized treatment in that radiation dose to the tumor can be increased while retaining normal tissue dose at a tolerable level.

Existing external beam radiotherapy treatment planning procedures are usually based on the definition of the tumor region on computed tomography (CT) images obtained in axial sections of the body. With the advent of magnetic resonance imaging (MRI) systems native, non-axial image planes were made feasible. Combined with the greatly enhanced soft-tissue contrast in MR images, several pathologic conditions are better visualized using this technique as compared to CT. The need for MR data in the radiotherapy process has been expressed in several publications. Modified tumor volume definitions using MR data as compared to CT have been reported in prostate carcinomas [22, 37, 38] and for brain and head-neck lesions [26, 27, 33, 36, 39, 41, 49, 50]. Discrepancies between MR and CT have been reported also at other tumor sites [39]. Although the intrinsic features of MR allow for a discrimination of tumor from surrounding normal tissue which is superior to CT in many types of cancer, the potential of using MR information in the treatment design is, however, not yet fully explored. This is mainly due to 2 reasons. Firstly, MR images are known to suffer from geometric distortions. Second is the lack of reliable techniques to convert the MR image signal to tissue-specific electron density information. Such tissue data are required in order to calculate the absorbed dose distribution from photon or charged particle irradiation of the tissue (calibrated from CT Hounsfield units in CT-based planning).

The majority of the MRI units used in diagnostic imaging are medium- to high-field superconducting systems (from 0.5 T). With the introduction of interventional MRI techniques that require easy access to the patient and a concurrent use of instruments (made from non-ferromagnetic materials) inside the magnet bore during image acquisition [7], there has been a renewed interest also in low-field MRI systems (based on resistive or permanent magnets). MRI units designed for interventional procedures based on an open magnet design that combines with a medium-to-low field magnet could offer advantages over conventional whole-body MRI systems also for imaging applications in radiotherapy. The open design concept allows for a patient to be imaged in the actual radiotherapy treatment position using individual immobilization devices. A low magnetic field is beneficial in interventional brachytherapy procedures, as susceptibility-induced artifacts from the applicators (MRI-compatible) increase at higher fields. The lower signal-to-noise and spatial resolution inherent to a low-field system compared to a high-field MR is, however, a significant drawback. Recently, a few manufacturers have announced open MR units working at higher fields (above 0.5 T). Provided these systems allow also for interventional procedures, they could provide a competitive alternative to the low-field open MR units in radiotherapy applications.

There is undoubtedly a growing interest in, and demand for, efficient procedures to incorporate MR image data in radiotherapy treatment planning. This was the topic of a recent review by Khoo et al. [24] in which they specifically emphasized the need for quality assurance procedures aimed at ascertain the geometric accuracy of the MR images. There are 2 major types of geometric distortions in MRI, i. e. those related to the performance of the imaging hardware (system-related), and those related to the magnetic properties of the imaged object (object-induced). The impact of these 2 types of distortion not only reflects the performance of the hardware, but also varies with magnetic field strength and with certain parameters of the imaging protocol. An understanding of these concepts will help to evaluate and correct for geometric distortions in MRI, and to define guidelines on how to compare systems from different manufacturers with regard to the requirements on geometric accuracy in radiotherapy.

The aim of this paper is to describe the basic issues related to geometric distortions in MR images, and to define situations where such distortions could influence the definition of the gross tumor volume in radiotherapy treatment planning. The paper is written mainly for physicists trained in radiotherapy but with only limited experience of MRI, and for oncologists using MR image data in radiotherapy treatment planning

procedures. The first part of this paper focuses on the origin and extent of geometric distortions in MRI. Both system-related and object-induced distortions are discussed, and their relative importance at different magnetic field strengths is outlined. Different distortion correction techniques and their limitations are reviewed. An overview of image registration techniques applicable to CT and MR image data sets is given in the second part of the paper. The sensitivity of different image registration techniques to the presence of geometric distortions in the MR data is discussed. A summary of image registration[3] techniques used and results obtained at some selected radiotherapy centers, is presented. The topic of mapping MR signals to electron densities is discussed in the last section.

Geometric Properties of MR Image Data

The Larmor equation is the fundamental equation in NMR, and relates the precession (Larmor) frequency of nuclear spins (ω) to the magnetic field ($\mathbf{B}$):

$$\omega = -\gamma \mathbf{B} \quad (1)$$

(The gyromagnetic ratio, γ, is a nuclei-specific constant. For protons the resonance frequency ($\omega/2\pi$) is 42.58 MHz at a field strength of 1.0 T).

The process of encoding spatial information in MRI is based on the Larmor equation (equation 1). In Fourier transform (FT) MRI, the encoding is accomplished by adding 3, linear magnetic field gradients to the main, static field during image acquisition. The effect is a spatial variation of the Larmor frequency of the tissue protons. During image reconstruction the magnetic field-related frequency and phase contents of the MR signals are translated into spatial positions. Consequently, disturbances in the magnetic field caused by a non-ideal hardware performance and/or the imaged object will cause mispositioning of structures.

System-Specific Distortion

The homogeneity of the static magnetic field ($\mathbf{B_0}$) generated by the imaging magnet is of utmost importance for the geometric properties of the MR data; it can be optimized by active and/or passive shimming. Active shimming is performed with special shim coils inserted in the magnet system. Passive shimming is achieved by introducing pieces of ferromagnetic metal around the magnet bore (tunnel). The 3 linear gradient magnetic fields used to spatially encode the different structures emitting MR signals, are generated by special gradient coils inserted into the bore of the magnet. Actively shielded gradient designs are often used in modern MRI units to reduce gradient non-linearity problems. In 2-D Fourier transform MR imaging, the formation of the MR signal is achieved by radiofrequency (RF) irradiation of the object in conjunction with the slice selection gradient, G_{slice}. This is referred to as selective excitation or slice selection, and is illustrated in Figure 1. The transfer of radiofrequency energy to the object (excitation) is achieved with the transmitter radiofrequency coil. The purpose of slice selection is to define which portion (i. e. slice) of the object will contribute to the MR signal. The slice selection gradient creates a range of Larmor frequencies in the object along the gradient direction. The bandwidth of the radiofrequency pulse restricts the excitation of protons to those having matching frequencies. The slice selection is followed by a spatial encoding in the image plane. For this purpose the phase encoding (G_{phase}) and frequency encoding (readout; G_{read}) gradients are applied during data preparation and acquisition, respectively. The measured MR signal (picked up by the receiver coil) originates from all signal-emitting structures within the selected slice, and corresponds to one setting of the phase encoding gradient (PE) amplitude. In order to collect data sufficient to reconstruct an image, the complete procedure from excitation to acquisition is repeated for a range of phase encoding gradient amplitudes (the spin warp technique); for instance, a 256 × 256 image matrix requires 256 signal measurements. Image reconstruction is performed after the data acquisition has been completed. The frequency and phase information in the MR signals is then used to map the data into the spatial domain. The reconstruction is based on a 2-D (or 3-D in case of 3-D-Fourier transform imaging) Fourier transformation of the data.

It can be concluded that hardware-related geometric distortions can be generated by a non-homogeneous static mag-

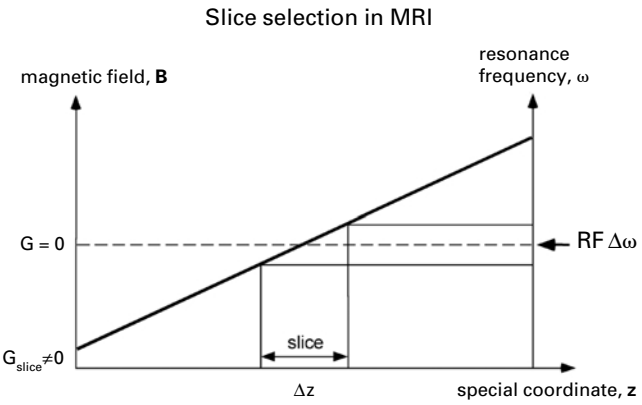

Figure 1. Selective excitation or slice selection refers to the combined application of a magnetic field gradient pulse (G_{slice}) and a shaped radiofrequency pulse (RF$\Delta\omega$). In this illustration, on-resonance irradiation of spins within a slice of thickness Δz is achieved with a radiofrequency pulse with bandwidth $\Delta\omega$.

Abbildung 1. Selektive Anregung oder Schichtselektion bezieht sich auf die kombinierte Applikation eines magnetischen Feldgradientenpulses (G_{slice}) und eines geformten Radiofrequenzpulses (RF$\Delta\omega$). In der vorliegenden Abbildung wird eine Bestrahlung der Spins in ihrer Resonanzfrequenz innerhalb einer Schicht der Dicke Δz erreicht mit einem Radiofrequenzpuls mit einer Bandbreite von $\Delta\omega$.

[3] In this paper "registration" refers to a coordinate transformation of one set of image data to match the second set of images. The term "image fusion" will be used in case an overlay of image information from 2 modalities is performed.

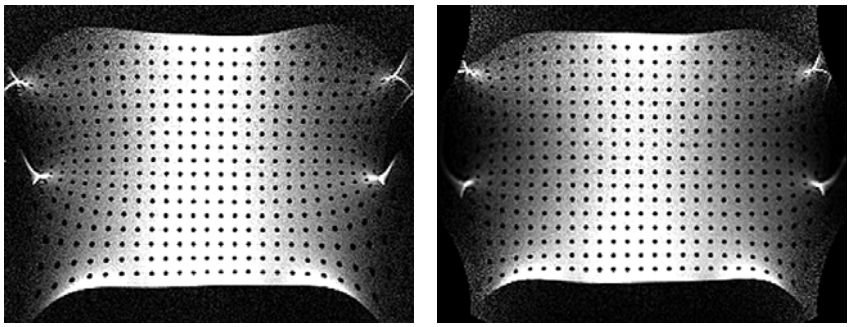

Figure 2. MR image (0.2 T) showing the typical "pillow-shaped" geometric distortion of a grid of equidistant tubes. The distance between tube centers is 1.5 cm. The left and right panels display, respectively, the distortion pattern before and after correction of in-plane distortion generated by static field inhomogeneity and gradient non-linearity using a technique provided by the manufacturer.

Abbildung 2. MR-Bild (0,2 T), das die typische kissenförmige geometrische Verzeichnung bei einem Raster von äquidistanten Röhren zeigt. Die Entfernung zwischen den Zentren der Röhren ist 1,5 cm. Der jeweils linke und rechte Teil der Abbildung zeigt das Maß der Verzeichnung vor und nach der Korrektur in der Ebene der Verzeichnung, die durch die Inhomogenität des statischen Feldes und die Nichtlinearität des Gradienten hergerufen wurde. Die Verzeichnungskorrektur basiert auf einer Technik, die vom Hersteller zur Verfügung gestellt wurde.

netic field, misadjusted amplitudes and non-linearity of the gradient fields (includes effects of eddy currents generated by the switching of gradients during image acquisition), and misadjustment of the radiofrequency (transmitter). The geometric distortions can appear both as slice position errors and as in-plane distortions in the MR images. In commercial MRI scanners, the 2 major sources of system-specific distortions originate from a non-linearity of the imaging gradients and from a non-homogeneous static field.

Evaluation: Geometric distortion generated by hardware can be evaluated from phantom measurements. For this purpose a combination of a grid that allows the evaluation of spatial misregistrations in the image plane (Figure 2), and a ramp (angled rod or plate along the direction of the slice selection gradient) to evaluate slice position errors, can be used [14]. For the evaluation of additional distortions of the imaged slice (i. e., slice tilt and warp), several sets of angled rods (plates) across the image plane are needed [32, 42]. In order to prevent interference of susceptibility-induced geometric uncertainties (discussed in section "Susceptibility") in the phantom MR data, the phantom(s) should be constructed from materials with matching susceptibility. For instance, with water-filled phantoms and for common gradient bandwidths used in MRI, this could be achieved with materials having susceptibilities within about ± 3 ppm (10^{-6}) from water [44]. The geometric properties of MR data produced with a certain clinical scanner should be evaluated for the complete set of imaging protocols used in clinical practice. It has to be emphasized that an evalua-tion of the distortion based on measurements using one image protocol is not necessarily representative of the performance using other protocols. This is related to that different imaging protocols can be defined with different bandwidths of the read-out gradient, having different slice selection gradient strengths, not being equally sensitive to eddy current effects, etc.

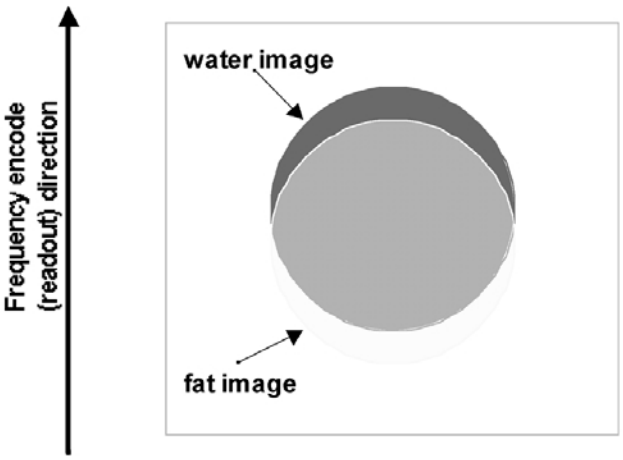

Figure 3. The signal from fat in adipose tissue will be displaced along the frequency encode direction in the MR image. This reflects the difference in resonance frequency between protons in water and fat (3.5 ppm).

Abbildung 3. Das Signal des Fettgewebes wird verschoben entlang der Frequenzkodierungsrichtung in dem MR-Bild. Dies basiert auf dem Unterschied in der Resonanzfrequenz zwischen Protonen in Wasser und Fett (3,5 ppm).

Object-Induced Distortion

Chemical Shift: Protons bound in carbon-hydrogen chains in adipose (fatty) tissue have slightly different resonance frequency than tissue water protons. This difference is about 3.5 ppm, or 150 Hz at 1.0 T. The spatial encoding process cannot distinguish the water and fat signals, and with the water frequency as the reference frequency, the signal from fat will be mispositioned. This chemical shift effect in fatty tissue is illustrated in Figure 3, showing an image originating from the water signal component, and an image corresponding to the fat signal component that is displaced along the frequency encode direction. Similar displacement of the signal from fat will occur also along the slice selection gradient.

Chemical shift effects are pronounced at higher magnetic fields. This is because the bandwidth of the readout gradient normally is insufficient to compensate for the increase (in Hz)

of the chemical shift observed at higher fields. For example, the chemical shift difference of water and fat is 30 Hz at 0.2 T and 220 Hz at 1.5 T. With a readout gradient bandwidth of 100 Hz/pixel, the chemical shift at 0.2 T amounts to 30/100 = 0.3 pixels, while at 1.5 T the fat signal will be displaced 220/100 = 2.2 pixels in the frequency encode (readout) direction. (Common pixel sizes in MRI are between 1×1 and 2×2 mm.) As an increase in the readout bandwidth causes a decrease in the signal-to-noise of the data due to an increased noise level, and this would remove one of the major benefits of high-field imaging, it is seldom used as a complete remedy to the problem. For instance, comparing an 0.2 T MR with a 1.5 T magnet from one specific manufacturer, the bandwidth per pixel defined for standard imaging protocols[4] is typically about a factor of 2 larger at the higher field. Using the example above, the chemical shift at 0.2 T (0.3 pixels; 100 Hz/pixel), should then be compared to a shift of approximately 1.1 pixel at 1.5 T (200 Hz/pixel), applying similar imaging protocols. This means that the distortion of fatty tissue due to chemical shift effects will be more pronounced at higher magnetic fields when similar pixel sizes are used. This can have implications in radiotherapy treatment planning in body regions with extensive fatty tissue contents, such as at the patient outline in abdominal examinations (subcutaneous fat). The effects of chemical shift can be deduced from the imaging parameters (readout bandwidth, FOV, image matrix, slice selection gradient).

Susceptibility: The susceptibility of a material is a measure of its ability to become magnetized when placed in an external magnetic field. As a result of the magnetization of the tissue, local field changes will occur at the interface between tissues with different susceptibilities. In MRI this will cause geometric distortions, as the magnetic field at a given spatial location will differ from the expected field strength at this location given by the main, static field and the gradient fields.

Susceptibility effects in vivo are pronounced at tissue-air interfaces, such as around the nasal cavities and along the patient outline, and susceptibility-generated field changes of up to ± 9 ppm can be introduced at such interfaces [44]. The estimation of susceptibility effects in MR images is complex due to the dependence on the shape and orientation of the object in the magnetic field. When phantom studies are performed to evaluate effects of susceptibility on the geometric accuracy of MR image data, care must therefore be taken to perform such studies under close patient-like conditions with regard to the imaged object (shape, orientation, composition). In similarity with chemical shift effects, susceptibility-induced distortions are pronounced at high fields and are directly linked to the bandwidth of the readout gradient. A rough estimate of the maximum position error is given by Schenk [44]:

$$\Delta x = \Delta\chi B_0 / G_{read} \quad (2)$$

With a susceptibility difference $\Delta\chi = 9 \times 10^{-6}$ at tissue-air interfaces, and G_{read} = 100 Hz/pixel, the maximum displacement in the readout direction in such regions of the image is about 0.8 pixels at 0.2 T, which is increased to about 5.7 pixels at 1.5 T (or 2.8 pixels with G_{read} = 200 Hz/pixel). It should be noted that this refers to the maximum distortion that could be expected, and that susceptibility effects in vivo in many cases will be smaller. Susceptibility-induced distortion is pronounced at the interface between 2 materials, and yields, in addition to spatial errors, a distortion of the shape of the object. Distortion of the signal intensity in the MR image close to such interfaces can also occur. Consequently, in high-field MRI a distortion (with regard to shape and intensity) and spatial displacement of tissue at the interface with air could occur in certain regions of the body.

With regard to susceptibility effects, patients having any foreign metallic object (medical implants, shell-splinter, etc.) in the body are of special concern in MRI. This is related to the enhanced susceptibility distortions that can occur close to such objects. As both spatial distortions and contrast alterations can occur, awareness of such effects is critical to the correct interpretation of the image data [19]. In some instances such foreign objects present contraindications to the MRI examination [47]. Susceptibility intensity distortions are pronounced in MR images acquired using the so-called gradient-echo technique (GE). In order to reduce the impact of such effects the MR signals can be acquired as spin-echoes, i. e. use spin-echo (SE) or fast spin-echo (FSE, TSE) image protocols.

Performance of Clinical MRI Scanners

Medium- to High-Field Systems: With regard to the geometric properties of MR images it is convenient to separate high- and low-field MR systems. Whole-body MR systems based on superconducting magnets operate in the medium- to high-field range (above approximately 0.5 T). The first generation of superconducting systems displayed severe system-related distortions [34], with typical spatial misregistrations of up to 10 to 15 mm at positions corresponding to the patient outline in abdominal examinations [1, 11].

The importance of a homogeneous static magnetic field for accurate spatial information in the image data is illustrated in Figure 4a, showing image distortions at 1.5 T at different field inhomogeneities. With the development of efficient magnet shim procedures (active and passive) combined with actively shielded gradient designs, hardware-related image distortions have been significantly reduced in modern, superconducting MRI units. Typical field inhomogeneities of ± 1 ppm (maximal deviation) within a 30 cm diameter sphere can be expected at 1.5 T. On the other hand, object-induced geometric distortions (susceptibility effects at tissue-air interfaces, chemical shift displacement of adipose tissue) are not affected by improved hardware design, and can generate significant spatial misregistrations in high magnetic field MR imaging [17, 44] as discussed in the previous section.

[4] In this case, "standard" imaging protocols refer to spin-echo (SE) or fast (or turbo) spin-echo (FSE; TSE) imaging protocols.

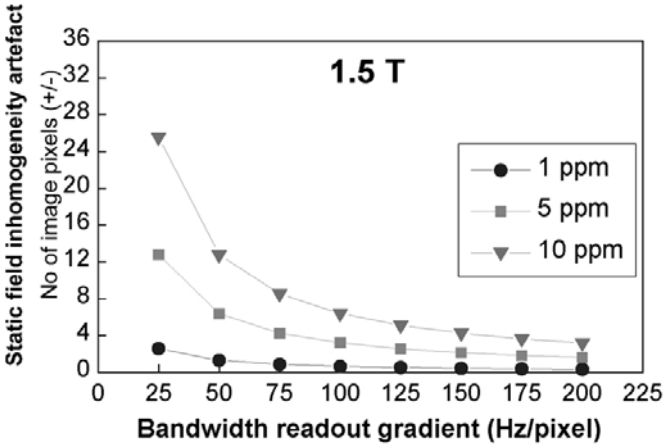

Figure 4a – Abbildung 4a

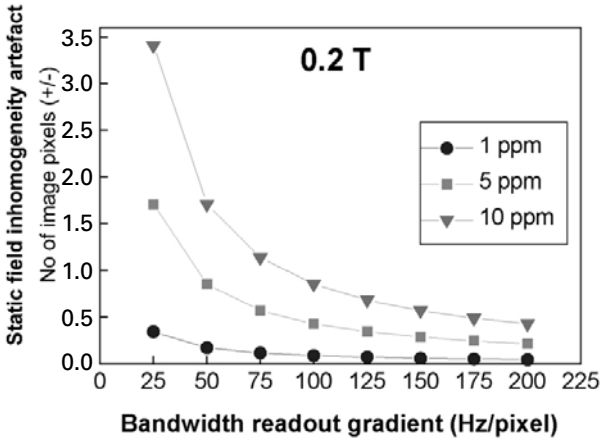

Figure 4b – Abbildung 4b

Figures 4a and 4b. Displacement of the MR signal along the readout (frequency encode) direction in the image for different field inhomogeneities at 1.5 T (a), and at 0.2 T (b). Note: the vertical axis of the 1.5 T data has a 1 order of magnitude larger scale compared to the 0.2 T data.

Abbildungen 4a und 4b. Verschiebung des MR-Signals entlang der Ausleserichtung (Frequenzkodierungsrichtung) im Bild für die verschiedenen Feldinhomogenitäten bei 1,5 T (a) und bei 0,2 T (b). Beachte: Die 1,5-T-Daten unterscheiden sich um etwa einen Faktor von 10 von den 0,2-T-Daten, jeweils bezogen auf die X-Achse.

Low-Field Systems: In the case of low-field systems (below approximately 0.5 T) different magnet designs are used, i. e. permanent or resistive magnets. Such magnets normally suffer from relatively large magnetic field inhomogeneities. Although modern coil designs and shim procedures have considerably improved the homogeneity of the static fields of such MR systems, field inhomogeneity (in ppm) is increased compared to superconducting systems, and is typically ± 5 ppm (maximal deviation) within a 30 cm diameter sphere in a resistive, low-field magnet. The effect of an inhomogeneous static field on the spatial accuracy at 0.2 T is illustrated in Figure 4b.

In the context of geometric accuracy of MR data, an additional, important distinction between high- and low-field MR systems is related to the impact of object-related distortions. While chemical shift artifacts and susceptibility distortions can cause significant spatial misregistrations at high fields, their impact on the MR data at lower fields is substantially reduced. This means that at fields below about 0.5 T, imaging sequences providing sufficient signal-to-noise can be defined such that the geometric distortions due to either of these object-related effects can be kept below about 1 to 2 pixels. This is achieved by defining a lower limit for the bandwidth of the readout gradient during image acquisition. Figures 5a and

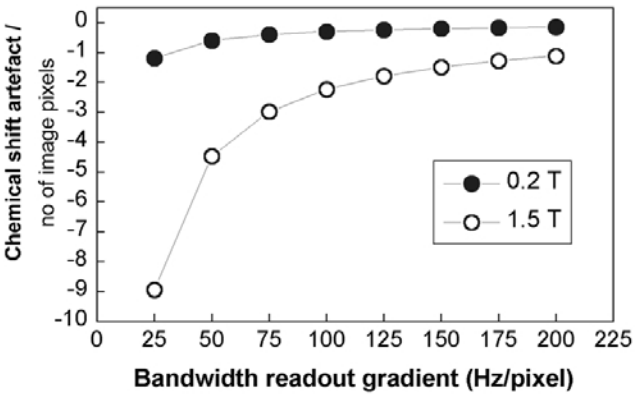

Figure 5a – Abbildung 5a

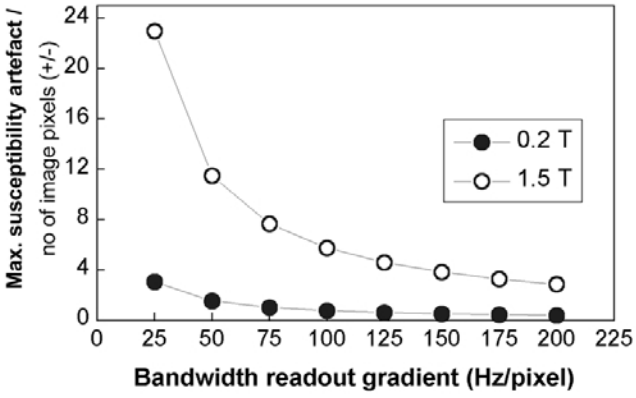

Figure 5b – Abbildung 5b

Figures 5a and 5b. Chemical shift (a) and maximum susceptibility artifact (i. e. 9 ppm [44]) expected in vivo (b) at 0.2 T and 1.5 T, plotted as a function of the bandwidth of the readout gradient.

Abbildungen 5a und 5b. Chemische Verschiebung (a) und maximaler Suszeptibilitätsartefakt (= 9 ppm [44]) (b), die bei 0,2-T- und 1,5-T-Geräten in vivo erwartet werden. Diese Parameter sind dargestellt als Funktion der Bandbreite des Auslesegradienten.

5b show the impact of object-related distortions on the MR data at 0.2 T compared to 1.5 T.

A last issue, common to both high- and low-field MR units is that system-related geometric distortions increase with distance from the magnet isocenter. This is related to elevated static field inhomogeneity and gradient non-linearity in such regions of the magnet. The distortion varies, most likely, with slice orientation and with imaging protocol, and should therefore be evaluated for the clinically relevant situations (protocol; orientation). As the distortion increases with distance from the magnet isocenter, the need for geometric correction schemes is pronounced when large image FOV are required. Object-induced distortions generally increase at higher magnetic fields. Specifically, it should be noted that the geometric accuracy of the MR data decreases with decreasing gradient bandwidth during data acquisition. High-bandwidth image protocols that are compatible with the signal-to-noise requirements of the MR images should therefore be used.

Procedures for Distortion Correction

Some manufacturers provide distortion correction procedures as part of their standard acquisition and evaluation software. A survey of such procedures indicates, however, that the correction in some cases only accounts for first-order non-linearity of the gradients, and/or is limited to specific acquisition settings. Furthermore, object-induced distortions are not accounted for by these procedures. In situations where such correction procedures are not sufficient to account for the distortion within the region of interest in the MR data, complementary techniques could be applied.

Phantom-based corrections of MRI distortions generated by limitations in the performance of the imaging hardware have been attempted using grid phantoms with known geometry [11, 31, 41, 42, 45]. Based on (distorted) images of the distribution of grid points measured at different slice positions and orientations in the magnet, correction polynomials have been defined and applied to rectify patient images acquired at corresponding positions, using identical imaging protocols and parameter settings. This approach allows a correction for geometric distortions in the image plane. In order to correct also for inaccuracies in slice definition (position, tilt, and warp), additional information based on image data of phantoms containing angled rods/plates is required [14, 32, 42].

A second, and maybe more sophisticated, approach to correct for system-specific geometric distortions is based on the acquisition of a magnetic field-map that combined with gradient non-linearity data can be used to restore the spatial information. Spatial displacement of the MR signal that originates from static field inhomogeneity and gradient non-linearity can with 2-D-Fourier transform imaging techniques be expressed as [1]:

$$\Delta z = \Delta \mathbf{B}_{grad,z}\,(x,y,z)/G_{slice} + \Delta \mathbf{B}_0(x,y,z)/G_{slice} \quad (3a)$$

$$\Delta y = \Delta \mathbf{B}_{grad,y}\,(x,y,z)/G_{phase} \quad (3b)$$

$$\Delta x = \Delta \mathbf{B}_{grad,x}\,(x,y,z)/G_{read} + \Delta \mathbf{B}_0(x,y,z)/G_{read} \quad (3c)$$

with z = slice selection direction, y = phase encoding direction, and x = frequency encode (readout) direction. The inhomogeneity of the static magnetic field, $\Delta \mathbf{B}_0$, creates a spatial displacement of the MR signal along the frequency encode direction in the image plane, and along the slice selection direction. The amplitudes of these distortions are related to the strength of the gradient fields along the x- and z-directions, respectively. Errors in the gradient fields, $\Delta \mathbf{B}_{grad}$, translate into spatial displacements in a similar way. It has been shown that geometric distortions related to the magnetic field $\mathbf{B}_0$ decrease with increasing gradient strength, while gradient-related distortions are virtually independent of the gradient strength [1]. The distortion generated by a non-homogeneous static magnetic field and gradient non-linearity can be deduced from phantom measurements, and used to shift a displaced image pixel to its correct position [1].

When an object (patient) is placed in the magnet the magnetic field will change slightly due to the susceptibility difference between the object and the surrounding air. Small field variations within the object attributed to susceptibility will also occur. In order to establish the magnetic field for subsequent distortion correction of patient data, the field distribution should preferably be evaluated under patient-like conditions. Special field-sensitive MR imaging techniques, such as the one proposed by Ericsson et al. [10], can be applied for this purpose. The outcome is a 3-D map of the magnetic field distribution within the object, and includes field distortions related to tissue susceptibility effects. Procedures based on such field-mapping techniques have been successfully applied to correct MR image data [48, 55]. Correction techniques based on "in vivo" field mapping can be extended to include also gradient non-linearity errors using equation 3.

Techniques that allow a correction also of chemical shift effects have been presented [3, 5]. The method proposed by Chang et al. [3] involves post-processing of duplicate image data sets acquired at 2 different readout gradient strengths (for instance by using a polarity reversal of the readout gradient in the second measurement). Errors in the position of structures along the readout direction in the image plane will be reversed in the second data set. The correct position can then be calculated from the 2 sets of images. This procedure allows for an in-plane (2-D) distortion correction. A more comprehensive 3-D version of the technique requires appropriate changes made also to the slice selection gradient for the acquisition of the second data set. The 2-D version of this technique has been successfully applied to MR imaging of the pelvis at high fields [11], and additionally used in a detailed study of the relative impact of system- and object-specific distortions at 1.5 T using typical clinical imaging protocols [31]. However, the drawback of the technique is the significantly prolonged acquisition time (doubled), and that it is prone to signal intensity artifacts in the corrected data set. Its use in clinical practice has therefore been limited.

An additional effect related to field inhomogeneities in MRI could be erroneous signal intensities in the image. Procedures to correct also for such anomalies of the data have been defined and successfully applied to clinical MR images [46, 55].

QA Program for Monitoring of MR System Performance

As the geometric properties of the MR data are closely linked to the status of the different hardware components (magnet, gradient, and radiofrequency systems), the long-term system performance should be monitored. In this way, the impact of system instabilities on the geometric accuracy and reproducibility of the image data can be evaluated.

Most vendors of MR systems provide quality assurance procedures within their standard data acquisition software. A set of phantoms for the evaluation of basic QA parameters is normally also supplied. In order to monitor the performance of the MR unit with regard to the geometric properties of the image data, the QA program should preferably provide information on the static field homogeneity and stability, gradient amplitude and linearity, stability in eddy current generation, and radiofrequency stability.

Registration of CT and MR Image Data

Registration Techniques

In order to fully utilize the superior soft tissue contrast in MR images for target definition in radiotherapy, a registration with the corresponding CT images is required. Image registration can be achieved at different levels of accuracy, mainly reflecting the extent of user-interaction and choice of registration technique. The field of image registration and registration-related segmentation is extensive [52]. This paper will focus on the techniques most commonly applied to match image data in radiotherapy treatment planning.

The majority of techniques used to register CT and MRI data assume that the imaged volume can be treated as a rigid body. A coordinate transformation based on translation, rotation, and linear scaling of the data sets can then be applied to correlate images from the 2 modalities. The transformation can be represented as a linear spatially invariant function of the form [23]:

$$\mathbf{r}_{study1} = \mathbf{A} \times \mathbf{r}_{study2} + \mathbf{b} \quad (4)$$

with **r** representing the coordinates of corresponding points in the 2 studies. The matrix **A** includes operations of rotation, scaling, and plane reflection; the vector **b** describes the operation of translation. Differences in patient set-up between the 2 studies is accounted for by the rotation, translation, and plane reflection parameters, while the scaling parameters are included to adjust "miscalibrations" of the imaging devices. In the case of MR, incorrect scaling in the images is attributed mainly to misadjustments of the gradients. The parameter values corresponding to a "best fit" of the 2 data sets is obtained by minimizing a function describing the geometric misregistration between the 2 studies.

Strictly, the assumption of a rigid body is only fulfilled provided non-linear geometric distortion of the MR data and organ motion during the MR and CT examinations can be disregarded. Another potential problem in radiotherapy is patient weight changes between the examinations, and changes in anatomy (tumor shrinkage, etc.) due to therapy. This points at more advanced registration techniques involving non-linear, "elastic" scaling of image regions in certain situations. It could be argued, however, that elastic scaling of MR images would remove the information related to organ motion inherent to the MR data. While these problems are pronounced for the abdomen, their impact on imaging of the skull is much reduced. Consequently, the majority of the reported clinical applications of image registration are based on head studies.

There are several practical issues that need to be considered in order to use multimodality image data in radiotherapy treatment planning procedures. These are related mainly to data I/O and to the geometric consistency between image data sets. With regard to data I/O, the images should preferably be available in a standard digital format (DICOM) for direct input to the dose-planning computer. The geometrical consistency of the data sets should be verified. This refers to the patient orientation and position, slice parameters (position, thickness, gap) and image parameters (pixel size, image matrix, magnification). These parameter values are stored in the header of the image files. In case a direct digital input of the images is not available, the image data could be digitized from film. However, the complete geometrical information needed might not always be traceable from a hard-copy exposure of the image on film. An additional drawback with the digitization process is the reduction in image quality.

An excellent overview of registration techniques applicable to medical image data has been given by Kessler et al. [23]. They discuss interactive techniques and methods based on point-, line-, and surface matching, all based on the assumption of a rigid body. The principles behind each of these techniques are carefully described, and the advantages and limitations of each method for clinical use are outlined.

Manual Registration Methods: The most elementary manual technique is a visual transfer of the target volume from one data set to the other. However, this can yield substantial inaccuracies in outlining of the target region on the second image data set. More advanced techniques involve interactive, computer-assisted, visually based translations, rotations, and scaling of the 2 data sets. The user interacts with both data volumes until a subjective "best fit" in 3-D is achieved [23]. A convenient tool using this latter technique is to simultaneously present the CT and MR images in an overlaid view (image fusion). The content of CT and MR information in this "synthetic" image view can then either be varied in the range 0 → 100% CT in combination with 100 → 0% MR ("gray scale fusion"), combined using pseudocoloring, or pre-

sented as an overlay of contour information extracted from one image data set and displayed on the second set of images ("contour overlays"; Figure 6). Following registration one set of images can be resliced to conform to the second set. In this way the 2 image series are displayed with the same slice orientation and position. With image fusion techniques the registration accuracy can be conveniently assessed by a visual comparison of the position of structures in the fused CT and MR images. As with all manual techniques, the outcome of the registration is, however, observer-dependent. Poor registration accuracy can be expected when the patient outline is used to register the data, especially when large image FOV are needed to cover the patient anatomy. This is related to elevated geometric distortions in MR images in such body regions and to "anatomical" changes in the patient (weight, tumor shrinkage, etc.) between the CT and MR examinations.

Landmark-Based Techniques: a) Point-based registration: Landmark-based techniques can use either external or object-specific (anatomic) landmarks. In point-based techniques, points corresponding to the same location in the 2 data sets are defined. These pairs of points are subsequently used to correlate the images using a least-squares fit algorithm. A minimum of 4 non-coplanar points defined in each image data set are required to define a transform that includes rotation, translation, and scaling in 3-D [23], although the optimal number of points probably are somewhat higher [9, 18, 23]. The presence of geometric distortion in the MR data is of special concern with techniques based on external markers. As already discussed in previous sections, MR distortions are pronounced at the patient outline due to a combination of both system- and object-related effects; the field in homogeneity and gradient non-linearity increases with the distance from the magnet isocenter, the chemical shift of fatty tissue will cause the patient outline to be distorted, susceptibility artifacts are important at tissue-air interfaces. A good illustration of the effects that can be observed in high-field imaging of the pelvis region has been given by Finnigan et al. [11]. They reported spatial mispositioning of external markers of up to 5 mm in relation to the patient outline using typical clinical imaging protocols and a 1.5 T MR unit, before geometric correction of the data was performed. Such systematic errors in the marker position relative to the patient anatomy will affect the registration accuracy, and call for distortion correction of the image data prior to registration. Another example is the registration of image data using stereotactic frames to correlate data from different image modalities. Spatial misregistrations of reference points in stereotactic frames of up to 2 to 3 mm, related mainly to susceptibility effects in MR images acquired with typical clinical image protocols, have been reported by Schad et al. [42].

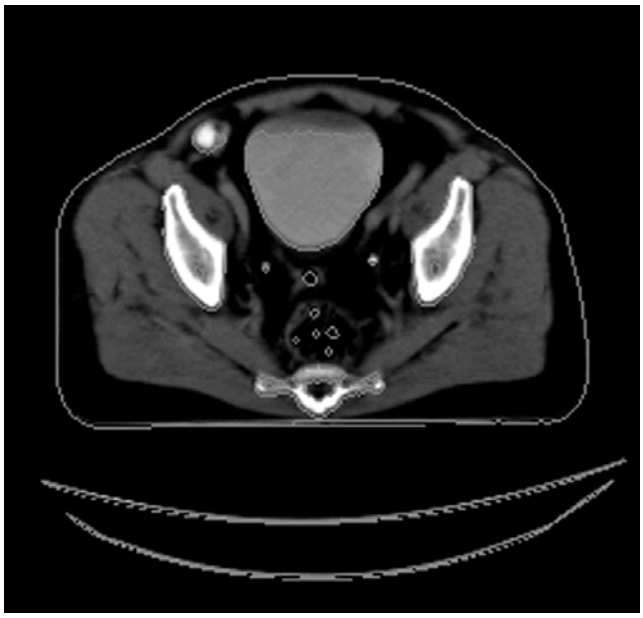

Figure 6. Image fusion using the technique of contour overlays of MRI data (outline of bony structures and bladder) onto registered CT images from a pelvis examination. The data sets were registered using a manual, interactive, rigid body technique.

Abbildung 6. Bildfusion basierend auf der Technik von Konturüberlagerungen von MR-Daten (Konturierung der knöchernen Strukturen und der Harnblase) auf registrierte CT-Bilder bei einem Becken-CT. Die Datensätze wurden registriert mit Hilfe einer manuellen interaktiven Technik, die von einem Modell der starren Körper ausgeht.

b) Surface matching: Techniques based on surface matching involve a segmentation[5] of the tissue surfaces to be registered. The degree of automation of these techniques depends on the segmentation method used to define the surfaces. An interesting example has been presented by Chen et al. [4]. Their technique, referred to as "fit a hat onto a head", is based on the segmentation of the outer skull in the 2 data sets. The transformation that minimizes the volume between the skull surfaces is then obtained. As the outer skull can be segmented based on relatively simple techniques, such as gray-level thresh-holding, the matching can be performed without user intervention.

Another technique that allows a high degree of automation is referred to as chamfer matching. It is based on the definition of points belonging to the same anatomical structure in both data sets, and requires an initial segmentation of those structures in the images. The registration is then performed based on the definition and optimization of a cost function which defines the goodness of a fit between the template (or chamfer) images and the second image data set. An interesting application using chamfer matching of bony structures in CT and MR data has been reported by van Herk et al. [53], and by Kooy et al. [25]. Contrary to what is generally thought

[5] "Segmentation" refers to the extraction of regions in the image that fulfill certain criteria with regard to properties such as signal amplitude, signal gradient etc.

to be a "weak point" of MRI, namely its poor visualization of bone, the signal void in MR images from cortical bone has been successfully used for image registration with this technique. As the bony anatomy provides a rigid body it can be regarded as an ideal landmark for registration of images from different modalities.

Feature-Based Registration: Techniques based on the extraction of features (or patterns) in the images have also been used to register CT and MR image data. A technique based on the correlation of geometrical features extracted using differential operators has been reported by van den Elsen et al. [51]. This method allows for a completely automated image registration.

Registration Accuracy

Although the evaluation of registration accuracy is complicated by the fact that a "true" answer is seldom known, attempts have been made to evaluate the performance of image registration methods on clinical data using various techniques.

The topographic relationship of structures defined in the MR and CT data sets, respectively, has been used to evaluate registration accuracy using image fusion of registered CT and MR images. As this technique provides a simultaneous display of the CT and MR information in an overlay mode, inconsistencies in the position of structures in the 2 data sets can be estimated visually [39, 50]. Evaluations based on phantom data and computer simulations have also been reported [18, 23, 53]. Such studies provide information on the performance of a given registration method with regard to accuracy, but will not adequately take into account effects of patient-related geometric distortion, organ motion, etc. inherent to the clinical situation. The results indicate large variations in accuracy. Using chamfer matching, close to 1 mm accuracy has been reported [53]. This should be compared to estimated registration errors in the centimeter range when a visually based transfer of regions from one data set to another is performed [39]. In general, as most registration techniques are based on the assumption of a rigid body, higher registration accuracy can be expected for head studies compared to abdominal examinations. Moreover, in situations where a global registration cannot be obtained, a local "best fit" close to the region of interest could be used to improve the registration outcome.

The evaluation of the registration accuracy with landmark techniques is a topic of some controversy. A commonly used definition of the registration error in landmark registration techniques is the root-mean-square (RMS) distance between corresponding landmarks. The error is then estimated only at the landmark locations, and is assumed uniform throughout the registered volume. However, it has been shown that the accuracy of the registration varies within the volume, and displays a dependence on the distribution of points/surface(s) used for registration in relation to the region of interest [12, 16]. Hemler et al. [16] reported larger residual errors inside the brain than at the skin surface using surface-based registration techniques of CT and MR data acquired on a cadaver (skull). Their results indicate a higher registration accuracy close to the registration points/surface(s). Contrasting results have been published by Fitzpatrick et al. [12]. They developed a model for the evaluation of registration accuracy with point-based registration techniques that yield an estimated target registration error (TRE). The target registration error refers to the distance between homologous points-of-interest (i. e., target points) other than the landmark points. Their results show that the minimum root-mean-square of the target points is obtained at the centroid of the configuration of landmark points, and that the error increases with distance from this point. Although these studies yield different results concerning the location of the minimum registration error with respect to the configuration of landmarks, both are consistent in that the root-mean-square misfit of the landmarks themselves is not a good measure of the registration accuracy at other points within the volume.

Clinical Applications of Image Registration in Radiotherapy Treatment Planning

Despite the difficulties to handle especially object-induced distortions, attempts have been made to register MR data with CT images for subsequent use in external beam dose planning procedures [13, 15, 18, 22, 25–27, 36, 37, 39–41, 49, 50]. In this section, an overview of techniques used and results reported by some radiotherapy centers that have been especially active in this field, is given.

Already in 1987 Fraass et al. [13] at the University of Michigan reported on the technical considerations that needed to be accounted for to integrate MRI data in radiotherapy treatment planning. Their UMPlan 3D TPS was used for image display and handling. The MR data were acquired at 0.35 T. Both the CT and MRI studies were performed with the patients immobilized in their treatment position. The registration of the CT and MR images was initiated with a fit of external markers. This procedure was then complemented with computer-assisted interactive translation and rotation of the images. Geometric distortions in the MR data was accounted for using an unwarping algorithm based on tie points defined in the CT and MR data. The tie points in the MR data were then forced to conform to the corresponding tie points in the geometrically accurate CT data. The registration accuracy was evaluated from contours extracted from one image data set (MR) and overlaid onto the registered set of images (CT). Moreover, 3-D surfaces of anatomical structure(s) defined in the MR data could be displayed on the CT data. In 1992, Thornton et al. [50] presented results obtained applying these techniques on patients with brain neoplasms. Patient MR data were acquired with units operating at 0.35 T, 0.5 T, or 1.5 T. An interactive rigid body 3-D surface matching of the brain parenchyma as defined by contours drawn in the CT and MR data, respectively, was introduced and additionally used to

register the CT and MRI data sets. No correction of MRI geometric distortion was reported. The registration accuracy was evaluated by a visual inspection of superimposed image data. Based on the results for 60 patients, they concluded that the CT-defined fields needed to be enlarged to encompass MRI tumor volumes for brain neoplasms, and that the CT and MRI data were complementary for the definition of tumor volume in these patients. In a parallel study from this group (Ten Haken et al. [49]), also published in 1992, the impact of interobserver variation on tumor volume definition in these patients was reported. They concluded that differences in tumor delineation between observers were similar in magnitude to the differences observed between image modalities, calling for histology studies to be performed in order to determine the significance of each modality in describing tumor volumes.

The group at the University of North Carolina at Chapel Hill has reported image registration of MRI and CT data using interactive image fusion techniques [40]. The image data were either digitized from film, or input directly in digital format to the fusion software. Although a variety of both manual and automated registration tools had been implemented, the most useful approach in their view was based on the fusion of images from arbitrary cut planes through the 2 3-D image data sets. Translations and rotations of transverse, sagittal, and coronal images were then used to register the data. The registration accuracy was evaluated from a visual inspection of fused images. In situations where complete anatomical registration could not be performed, they focused on a local registration of the region of major interest. Following registration, the transformation matrix was entered into their PLan UNC 3D TPS and used to perform a pixel-mapping of the second image data set to conform with the "planning" CT data. In this way, information from the second set of images was made available to the TPS, and could be correctly projected into all aspects of the treatment plan. In a recent retrospective study of 246 patients undergoing 3-D treatment planning at their institute from mid 1994 to end 1995, they reported that 106 (43%) had had image registration between the planning CT and a second, non-planning CT, or an MRI examination [39]. Tumor sites represented in the study were brain, head-neck, thorax, abdomen, pelvis, and extremities. Their results indicated a change in tumor location in the treatment plan of a minimum of 1.5 cm for 50% of these patients, and up to 3 cm for 25% of the patients, compared to using only the planning CT data. This group has not reported any distortion correction of the MR data prior to registration, and has claimed that the effect of geometric inaccuracies in the MR data has not been convincingly observed under clinical work conditions in their institution [39]. Details on the magnet field strengths corresponding to the MRI data used for image registration have neither been reported.

Clinical results based on chamfer matching of internal bony structures in CT and MRI (1.5 T) data have been reported by groups at the Netherlands Cancer Institute and the Institute of Cancer Research and The Royal Marsden NHS Trust, [26, 36, 37]. After extraction of bony structures in the 2 data sets, a best "chamfer" fit was defined and applied to automatically match the images using translation, rotation, and scaling of the data. The technique has been applied to patients with brain cancer [26], head-neck cancer [36], and prostate carcinoma [37]. For brain lesions (base of skull meningiomas) the MR target volumes were found to be larger but not inclusive of the corresponding CT volumes; for head-neck cancer the MR-defined tumor volumes were smaller and with less interobserver variation compared to CT; for prostate carcinoma the MR-defined prostate volumes were smaller than with CT. Apart from allowing linear scale corrections of the image data, no geometric distortion correction of the MR images was reported in these studies. Taking into account the position of the bony structures (in relation to the patient outline and to interface with air), the impact of object-induced distortion in the MR images on the registration outcome should be of minor importance.

The groups at the German Cancer Research Center and University of Heidelberg have developed techniques to integrate MRI into stereotactic radiotherapy procedures of patients with lesions in the head and neck region [8, 15, 41]. In a study including 195 patients, a stereotactic frame attached to the patient's head was applied during imaging (CT, MRI) and irradiation [15]. System-induced geometric distortion in the MRI data was accounted for by separate phantom evaluations, followed by a correction based on polynomial modeling of the distortion pattern. The registration of the CT and MR images (distortion-corrected) was based on 12 frame marker points. The results of this study indicated increased tumor volumes in 2/3 of the patients using MRI.

The techniques used and the results obtained in these studies are summarized in Table 1.

Applications in extracranial, stereotactic radiotherapy have also been reported. The group at the Karolinska Hospital in Stockholm has developed a stereotactic body frame that can be used in CT, MR and PET scanners [28]. As the markers are placed far from the magnet isocenter in a MR examination, the use of such markers for image registration of abdominal images will require a careful assessment of the geometric accuracy of the image data in these regions of the magnet.

Another interesting approach to the use of MRI data in radiosurgical treatment planning was presented in 1994 by the group at the German Cancer Research Center in Heidelberg. They used the MRI data (1.5 T) as direct input to the dose calculation procedure by assuming a homogeneous attenuation value inside the head [43]. A stereotactic localization frame was used both during MR imaging and irradiation. Correction for system-specific distortion reduced the error in the position of the stereotactic frame coordinates from about 2 to 3 mm to 1 mm (= pixel size). No correction for object-induced distor-

Anatomical region [Study]	Registration method	Evaluation	Magnetic field	Distortion correction	Results
Brain (60 patients) [50]	Interactive, rigid body: translation and rotation	Visual: superimposed brain surface contours	0.35 T 0.5 T 1.5 T	No	MRI tumor volumes larger than CT
Brain, head-/neck, thorax, abdomen, pelvis, extremities (106 patients) [39]	Interactive, rigid body: translation and rotation	Visual: fusion of images from arbitrary cut planes	Not reported	No	Change in tumor location with MRI – min. 1.5 cm in 50% of patients
a) Head-/neck (6 patients) [36] b) Prostate (18 patients) [37]	Chamfer matching, rigid body: translation, rotation, scaling (study b only reports translation and rotation)	Visual: image fusion	a) 1.5 T b) Not reported	a) Only linear gradient errors. b) No	a) MRI tumor volumes smaller and with less interobserver variation than CT b) Prostate volumes smaller with MRI
Brain (7 patients) [26]	2-steps: 1. Least squares fit of anatomical points; 2. Chamfer matching, rigid body: translation, rotation, scaling	Visual: image fusion Quantitative: anatomical points	1.5 T	Only linear gradient errors	MRI target volumes larger but not inclusive of CT volumes
Head-/neck (195 patients) [15]	Stereotactic registration, rigid body: translation, rotation	Minimization of RMS error of 12 external marker points	1.5 T	Phantom-based correction of system-specific distortion	MRI volumes larger than CT in 2/3 of patients

Table 1. A summary of techniques used and results obtained in some selected, clinical studies based on image correlation of CT and MRI data in radiotherapy treatment planning applications.

Tabelle 1. Zusammenfassung der in selektionierten klinischen Studien verwendeten Techniken, die sich auf eine Bildkorrelation von CT- und MR-Daten stützen und im Rahmen der Radiotherapie zur Anwendung kommen, und die erzielten Resultate.

tion was performed. Instead, the parameters of the MR imaging sequence were chosen so as to reduce the impact of such effects on the geometric accuracy of the image data. They reported a difference in dose estimation between the MRI-based dose planning and conventional CT planning of less than 2%.

In a recent study based on MRI data acquired at 1.5 T, it was argued that distortion-correction of brain MR images is not required for conventional radiotherapy, provided image acquisition is performed using high-bandwidth spin-echo protocols, and a small image FOV is used (that is, the imaged region is close to the magnet isocenter) [2]. This group also reported that 20 patients had had treatment plans based on MRI alone in their institute, by assuming a homogeneous attenuation value inside the head.

Clinical applications of image correlation in radiotherapy treatment planning based on the registration of anatomical point-pairs have also been presented [18, 22, 27], suggesting the CT and MR examinations to be complementary in radiotherapy treatment planning. Although no correction for distortion in the MR data (obtained at fields in the range of 1.0 to 1.5 T) had been performed in any of these studies, highly accurate registration results were reported (registration errors of about 1 to 2 mm).

As a final remark it should be pointed out that, until now, a significant fraction of the published studies in this field are based on data from "first generation" medium- to high-field MR systems. Consequently, both system- and object-induced distortions can be expected to have an impact on the geometric accuracy of the MR image data. In cases where no or only partial distortion correction has been performed, reported discrepancies between tumor volumes defined in registered CT and MR images, respectively, could therefore be affected by errors related to the geometric characteristics of the MR data. It can then be argued that the real impact of geometric distortions on the accuracy in target outlining based on registered MRI and CT data is not yet disclosed, and that further studies are needed in this field.

Future Developments Related to the Use of MRI in Radiotherapy Treatment Planning Procedures

Mapping of MR Data to Electron Density Information

Although the task of image registration of CT and MR image data is very cumbersome and prone to errors, there are no published results on the mapping of MR data to electron density information. Such a mapping would circumvent the need for CT-MR registration, as the MR data could be used directly as

the basis for dose calculation in radiotherapy. Unfortunately there is no direct link between tissue electron density data (calibrated from the CT Hounsfield units in radiotherapy treatment planning procedures) and MR signal amplitudes. Instead the MR signal mainly reflects the dynamics of tissue water, and is related to the density of protons in tissue water and to their relaxation properties (T1 and T2).

A possible approach to map the MR data – corrected for geometric distortion – to electron density information could be based on an initial voxel-based segmentation of the images into different tissue types followed by an assignment of bulk tissue electron densities to voxels representing the same tissue type. Segmentation of MR images are, however, often hampered by signal non-uniformities within the sensitive volume of the MR receiver coil [17, 24]. As a result, the MR images display signal non-uniformities that are not tissue-related [6, 29, 30]. Provided the stochastic component of the signal variation is small, its effect on the MR images can be modeled and corrected for using normalization techniques. Significant improvements in signal uniformity characteristics of MR image data have been reported using intensity correction or normalization techniques [6, 21, 30, 54]. Such techniques might also be useful to segment MR image data into tissue regions for dose-planning purposes.

Following a translation of the MR data into bulk tissue electron densities, a comparison of dose distributions obtained using CT or the converted MR data could be performed to evaluate the feasibility of using MR data as direct input to the dose calculation procedure. As already mentioned, such comparative studies have been performed on the brain with a homogenous attenuation value assigned to the MR data [2, 43]. As expected, insufficient accuracy is obtained in situations when the beam passes through internal air cavities in the skull, indicating that more refined techniques are needed that take into account tissue heterogeneity [2].

MR-Based Digitally Reconstructed Radiographs

To facilitate further a completely MRI-based treatment planning, techniques that allow the reconstruction of digitally reconstructed radiographs based on the MR image data have been presented [35, 56]. An interesting approach was discussed by Ramsey et al. [35]. They described a method based on the assignment of electron density information to the MR data, yielding MR-digitally reconstructed radiographs similar to the CT-based radiograph reconstructions. Although artifacts related mainly to the overlap of MR signal amplitudes in air and bone, respectively, distorted the MR-digitally reconstructed radiographs, the technique could potentially be improved with additional image processing prior to the generation of the digitally reconstructed radiographs. Further developments and refinement of such techniques will be necessary in order to replace CT by MR also in this step of the radiotherapy treatment planning process.

Conclusions

MR hardware-related distortions usually increase with distance from the magnet isocenter, and the need for geometric correction of the images (can be evaluated from measurements on phantoms) is therefore pronounced when a large image field-of-view is required. The distortions induced by the object (i. e., patient) increase at higher magnetic fields. These distortions cannot be evaluated from phantom data, and require relatively sophisticated correction techniques based on additional MR measurements performed directly on the patient. Both types of distortion decrease with an increased bandwidth during data acquisition. High-bandwidth image protocols that are compatible with the signal-to-noise requirements of the MR images should therefore be used. As the geometric properties of the MR data are closely linked to the performance of the different hardware components (magnet, gradient and radiofrequency systems), the long-term system performance should be monitored within the frame of a quality assurance program.

The majority of registration techniques used to match CT and MR image data sets are based on the assumption that the patient can be represented as a rigid body. This assumption is only valid provided non-linear geometric distortion of the MR data and organ motion during the MR and CT examinations can be disregarded. Taking into account the geometric properties of the MR data, it can be concluded that mispositioning of structures in the MR images most likely will be pronounced at the patient outline. Registration techniques based on external landmarks placed on the skin, surface matching of the skin surface, or use of stereotactic frames, are therefore especially sensitive to the presence of geometric inaccuracies in the MR data. It can be argued that bony structures, on the other hand, are relatively robust landmarks in the registration of image data; they (almost) fulfil the assumption of a rigid body, bones are usually not subjected to object-induced distortion, and they are normally situated at a distance from the patient outline.

In most published studies on image registration of CT and MR images in radiotherapy treatment planning the effects of geometric distortion on the outcome of the image match and the related error in the definition of the gross tumor volume are not discussed. It can therefore be concluded that further studies evaluating the impact of MR distortions on the outcome of image registration procedures are needed.

Note added in proof: Treatment planning based on MR images by mapping the MR data to a set of standardized, tissue-specific CT Hounsfield values prior to the dose calculation has recently been reported by Fransson et al. (Radiother Oncol 2000;56:Suppl 1:517).

Acknowledgement: The economical support from the Jubiläumsfond of the Austrian National Bank (project no 7764) is gratefully acknowledged. The support from M. Sc. Tomas Lorang, University of Vienna, Austria, in providing the image fusion results shown in Figure 6, and from Ass. Prof. Anders Ericsson, Uppsala University, Sweden, for suggesting the design of Figure 1, is gratefully acknowledged.

References

1. Bakker CJG, Moerland MA, Bhagwandien R, et al. Analysis of machine-dependent and object-induced geometric distortion in 2D FT MR imaging. Magn Reson Imag 1992;10:597–608.
2. Beavis AW, Gibbs P, Dealey RA, et al. Radiotherapy treatment planning of brain tumours using MRI alone. Br J Radiol 1998;71:544–8.
3. Chang H, Fitzpatrick JM. A technique for accurate magnetic resonance imaging in the presence of field inhomogeneities. IEEE Trans Med Imag 1992; 11:319–29.
4. Chen GTY, Pelizzari CA. Image correlation techniques in radiation therapy treatment planning. Comp Med Imag Graph 1989;13:235–40.
5. Cho ZH, Kim DJ, Kim YK. Total inhomogeneity correction including chemical shifts and susceptibility by view angle tilting. Med Phys 1988;15: 7–11.
6. Dawant BM, Zijdenbos AP, Margolin RA. Correction of intensity variations in MR images for computer-aided tissue classification. IEEE Trans Med Imag 1993;12:770–81.
7. Debatin JF, Adams G, eds. Interventional Magnetic Resonance Imaging. Berlin–Heidelberg–New York: Springer, 1998.
8. Ehricke H-H, Schad LR. MRA-guided stereotactic radiation treatment planning for cerebral angiomas. Comp Med Imag Graph 1992;16:65–71.
9. Ende G, Treuer H, Boesecke R. Optimization and evaluation of landmark-based image correlation. Phys Med Biol 1992;37:261–71.
10. Ericsson A, Weis J, Hemmingsson A, et al. Measurement of magnetic field variations in the human brain using a 3D-FT multiple gradient echo technique. Magn Reson Med 1995;33:171–7.
11. Finnigan DJ, Tanner SF, Dearnley DP, et al. Distortion-corrected MR images for pelvic radiotherapy treatment planning. Proc 19th L H Gray Conf 1997; Chapt 3:72–6.
12. Fitzpatrick JM, West JB, Maurer CR. Predicting error in rigid-body point-based registration. IEEE Trans Med Imag 1998;17:694–702.
13. Fraass BA, McShan DL, Diaz RF, et al. Integration of magnetic resonance imaging into radiation therapy treatment planning: I Technical considerations. Int J Radiat Oncol Biol Phys 1987;13:1897–908.
14. Fransson A, Prodinger R, Gerstner N, et al. System-specific geometric distortions in MR images from a 0.2 T resistive MRI unit. Radiother Oncol 1998;48:S187.
15. Gademann G, Schlegel W, Debus J, et al. Fractionated stereotactically guided radiotherapy of head and neck tumors: a report on clinical use of a new system in 195 cases. Radiother Oncol 1993;29:205–13.
16. Hemler PF, Napel S, Sumanaweera TS, et al. Registration error quantification of a surface-based multimodality image fusion system. Med Phys 1995; 22:1049–56.
17. Henkelman RM, Bronskill MJ. Artifacts in magnetic resonance imaging. Rev Magn Reson Med 1987;2:1–126.
18. Hill DLG, Hawkes DJ, Gleeson MJ, et al. Accurate frameless registration of MR and CT images of the head: applications in planning surgery and radiation therapy. Radiology 1994;191:447–54.
19. Hosten N, Wust P, Beier J, et al. MRI-assisted specification/localization of target volumes Aspects of quality control. Strahlenther Onkol 1998;174: Suppl II:13–8.
20. ICRU International Commission on Radiation Units and Measurements. Prescribing recording and reporting photon beam therapy. Report ICRU 50. Bethesda, MD: ICRU, 1993.
21. Johansson SA, Magnusson P, Fransson A, et al. Improvements in absorbed dose measurements for external radiation therapy using ferrous dosimeter gel and MR imaging (FeMRI). Phys Med Biol 1998;43:261–76.
22. Kagawa K, Lee WR, Schultheiss TE, et al. Initial clinical assessment of CT-MRI image fusion software in localization of the prostate for 3D conformal radiation therapy. Int J Radiat Oncol Biol Phys 1997;38:319–25.
23. Kessler ML, Pitluck S, Petti P, et al. Integration of multimodality imaging data for radiotherapy treatment planning. Int J Radiat Oncol Biol Phys 1991;21:1653–67.
24. Khoo VS, Dearnaley DP, Finnigan DJ, et al. Magnetic resonance imaging (MRI): considerations and applications in radiotherapy treatment planning. Radiother Oncol 1997;42:1–15.
25. Kooy HM, van Herk M, Barnes PD, et al. Image fusion for stereotactic radiotherapy and radiosurgery treatment planning. Int J Radiat Oncol Biol Phys 1994;28:1229–34.
26. Khoo VS, Adams EJ, Saran F, et al. A comparison of clinical target volumes determined by CT and MRI for radiotherapy planning of base of skull meningiomas. Int J Radiat Oncol Biol Phys 2000;46:1309–17.
27. Lattanzi JP, Fein DA, McNeeley SW, et al. Computed tomography magnetic resonance image fusion: a clinical evaluation of an innovative approach for improved tumor localization in primary central nervous system lesions. Radiat Oncol Invest 1997;5:195–205.
28. Lax I, Blomgren H, Näslund I, et al. Stereotactic radiotherapy of malignancies in the abdomen. Acta Oncol 1994;33:677–83.
29. Lerski RA, McRobbie DW, Straughan K, et al. Multicenter trial with protocols and prototype test objects for the assessment of MRI equipment. Magn Reson Imag 1988;6:201–14.
30. McVeigh ER, Bronskill MJ, Henkelman RM. Phase and sensitivity of receiver coils in magnetic resonance imaging. Med Phys 1986;13:806–14.
31. Moerland MA, Beersma R, Bhagwandien R, et al. Analysis and correction of geometric distortions in 1.5 T magnetic resonance images for use in radiotherapy treatment planning. Phys Med Biol 1995;40:1651–64.
32. Podo F, Orr JS, Schmidt KH, et al. IV Protocols and test objects for the assessment of MRI equipment. Magn Reson Imag 1988;6:195–9.
33. Pötter R, Heil B, Schneider L, et al. Sagittal and coronal planes from MRI for treatment planning in tumours of brain head and neck: MRI assisted simulation. Radiother Oncol 1992;23:127–30.
34. Prott FJ, Haverkamp U, Willich N, et al. Comparison of imaging accuracy at different MRI units based on phantom measurements. Radiother Oncol 1995;37:221–4.
35. Ramsey CR, Oliver AL. Magnetic resonance imaging based digitally reconstructed radiographs virtual simulation and three-dimensional treatment planning for brain neoplasms. Med Phys 1998;25:1928–34.
36. Rasch C, Keus R, Pameijer FA, et al. The potential impact of CT-MRI matching on tumor volume delineation in advanced head and neck cancer. Int J Radiat Oncol Biol Phys 1997;39:841–8.
37. Rasch C, Barillot I, Remeijer P, et al. Definition of the prostate in CT and MRI: a multi-observer study. Int J Radiat Oncol Biol Phys 1999;43: 57–66.
38. Roach M, Faillace-Akazawa P, Malfatti C, et al. Prostate volumes defined by magnetic resonance imaging and computerized tomographic scans for three-dimensional conformal radiotherapy Int J Radiat Oncol Biol Phys 1996;35:1011–8.
39. Rosenman JG, Miller EP, Tracton G, et al. Image registration: an essential part of radiation therapy planning. Int J Radiat Oncol Biol Phys 1998;40: 197–205.
40. Sailer SL, Rosenman JG, Soltys M, et al. Improving treatment planning accuracy through multimodality imaging. Int J Radiat Oncol Biol Phys 1996; 35:117–24.
41. Schad LR, Gademann G, Knopp M, et al. Radiotherapy treatment planning of basal meningiomas: improved tumor localization by correlation of CT and MR imaging data. Radiother Oncol 1992;25:56–62.
42. Schad L, Lott S, Schmitt F, et al. Correction of spatial distortion in MR imaging: a prerequisite for accurate stereotaxy. J Comput Assist Tomogr 1987; 11:499–505.
43. Schad LR, Blüml S, Hawighorst H, et al. Radiosurgical treatment planning of brain metastases based on a fast three-dimensional MR imaging technique. Magn Reson Imag 1994;12:811–9.
44. Schenk JF. The role of magnetic susceptibility in magnetic resonance imaging: MRI magnetic compatibility of the first and second kinds. Med Phys 1996;23:815–50.
45. Schubert K, Wenz F, Krempien R, et al. Integration of an open magnetic resonance scanner in therapy simulation and three-dimensional radiation treatment planning. Strahlenther Onkol 1999;175:225–31.
46. Sekihara K, Kuroda M, Kohno K. Image restoration from non-uniform magnetic field influence for direct Fourier NMR imaging. Phys Med Biol 1984; 19:15–24.
47. Shellock F, Kanal E. Magnetic resonance: bioeffects safety and patient management. New York: Raven, 1994.
48. Sumanaweera TS, Glover G, Binford TO, et al.. MR susceptibility misregistration correction. IEEE Trans Med Imag 1993;12:251–9.
49. Ten Haken RK, Thornton AF, Sandler HM, et al. A quantitative assessment of the addition of MRI to CT-based 3-D treatment planning of brain tumors. Radiother Oncol 1992;25:121–33.

50. Thornton AF, Sandler HM, Ten Haken RK, et al. The clinical utility of magnetic resonance imaging in 3-dimensional treatment planning of brain neoplasms. Int J Radiat Oncol Biol Phys 1992;24:767–75.
51. van den Elsen PA, Maintz JBA, Pol E-JD, et al. Automatic registration of CT and MR brain images using correlation of geometrical features. IEEE Trans Med Imaging 1995;14:384–96.
52. van den Elsen PA, Pol EJD, Viergever MA. Medical image registration – a review with classification. IEEE Eng Med Biol 1993;12:26–39.
53. van Herk M, Kooy HM. Automatic three-dimensional correlation of CT-CT, CT-MRI and CT-SPECT using chamfer matching. Med Phys 1994;21:1163–78.
54. Vokurka EA, Thacker NA, Jackson A. A fast model independent method for automatic correction of intensity nonuniformity in MRI data. J Magn Res Imag 1999;10:550–62.
55. Weis J, Ericsson A, Silander HC, et al. Magnetic resonance spectroscopic imaging for visualization and correction of distortions in MRI: high precision applications in neurosurgery. Magn Reson Imag 1998;16:1265–72.
56. Yin FF, Gao Q, Xie H, et al. MR image-guided portal verification for brain treatment field. Int J Radiat Oncol Biol Phys 1998;40:703–11.

Address for Correspondence
Dr. Annette Fransson
Department of Radiotherapy and Radiation Biology
University Hospital – AKH/3B
Währinger Gürtel 18–20
A-1090 Vienna
Austria
Phone (+43/1) 404002-655, Fax -693
e-mail: A.Fransson@bmtp.akh-wien.ac.at